JACS
JOURNAL OF THE AMERICAN CHEMICAL SOCIETY
Article
pubs.acs.org/JACS

Potential-Dependent Electrocatalytic Pathways: Controlling Reactivity with pK_a for Mechanistic Investigation of a Nickel-Based Hydrogen Evolution Catalyst

Eric S. Rountree and Jillian L. Dempsey*

Department of Chemistry, University of North Carolina, Chapel Hill, North Carolina 27599-3290, United States

Supporting Information

ABSTRACT: A detailed mechanistic analysis is presented for the hydrogen evolution catalyst $[Ni(P^{Ph}_2N^{Ph}_2)_2(CH_2CN)][BF_4]_2$ in acetonitrile ($P^{Ph}_2N^{Ph}_2$ = 1,3,5,7-tetraphenyl-1,5-diaza-3,7-diphosphacyclooctane). This complex has a $Ni^{II/I}$ redox couple at −0.83 V and a $Ni^{I/0}$ redox couple at −1.03 V versus $Fc^{+/0}$. These two closely spaced redox events both promote proton reduction catalysis, each via a distinct mechanism: an electrochemical ECEC pathway and an EECC route. The EECC mechanism, operative at more negative potentials, was isolated through use of a weak acid (anilinium, pK_a = 10.6 in CH_3CN) to avert protonation of the singly reduced species. Electroanalytical methods and time-resolved spectroscopy were used to analyze the kinetics of the elementary steps of hydrogen evolution catalysis. The rate constant for the formation of a nickel(II)−hydride intermediate was determined via measurements of peak shift ($k_1 = 1.2 \times 10^6$ M^{-1} s^{-1}) and through foot-of-the-wave analysis ($k_1 = 6.5 \times 10^6$ M^{-1} s^{-1}). Reactivity of the isolated hydride with acid to release hydrogen and regenerate the nickel(II) complex was monitored by stopped-flow spectroscopy. Kinetics obtained from stopped-flow measurements are corroborated by current plateau analysis of the catalytic cyclic voltammograms. These kinetic data suggest the presence of an off-cycle intermediate in the reaction.

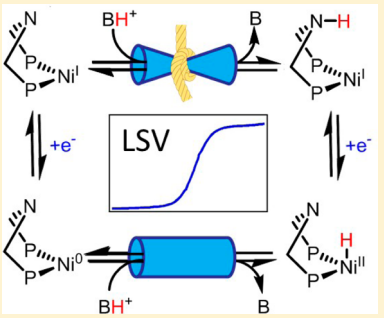

INTRODUCTION

With the search for sustainable energy becoming increasingly imperative, many researchers have turned their focus to molecular electrocatalysis to evaluate methods by which fuel production can be driven by renewable energy sources. Several reactions have been targeted in this effort, including water oxidation, hydrogen evolution, and carbon dioxide reduction.[1−5] The simplest of these reactions is hydrogen formation, as it is just a two proton−two electron process (eq 1), but even this has proven difficult to mediate efficiently with transition metal-based catalysts.

$$2H^+ + 2e^- \rightleftharpoons H_2 \quad (1)$$

The $[Ni(P^R_2N^{R\prime}_2)_2]^{2+}$ class of molecules, which can mediate both proton reduction and hydrogen oxidation, has played an important role in advancing the field of molecular hydrogen evolution catalysts thus far.[2,6−14] In these complexes, $P^R_2N^{R\prime}_2$ refers to a generic ligand set of the form 1,5-R′-3,7-R-1,5-diaza-3,7-diphosphacyclooctane, which contains two coordinating phosphines and two noncoordinating amines that are postulated to promote proton shuttling to and from the metal center. Studies of the role of the pendant amines and ligand electronics for these molecules have given meaningful insight into structure−activity relationships and the role of the secondary coordination sphere.[7,15−18] This understanding has already guided the design of increasingly efficient and fast hydrogen evolving catalysts.[7,8,11,19]In addition to the synthetic preparation of these catalysts and the quantification of their catalytic activity, it is of significant interest to understand the mechanisms by which hydrogen is evolved and to quantify the rate constants associated with the elementary steps. The catalytic reduction of protons to dihydrogen by a transition metal complex can occur through various mechanisms that differ by the sequence of the electron transfer steps (reduction of the catalyst or intermediates, denoted E) and the homogeneous chemical steps (protonation steps, denoted C). Several possible pathways for hydrogen evolution and their corresponding electrochemical analyses have been recently outlined by Costentin and Savéant.[20] By considering the individual elementary steps, one can envision perturbing the pathway of hydrogen evolution by varying parameters such as the strength of the acid employed and the applied potential. The $[Ni(P^R_2N^{R\prime}_2)_2]^{2+}$ class of molecules is an excellent example of this tunable reactivity. The $Ni^{II/I}$ and $Ni^{I/0}$ redox couples are generally both reversible and tend to be spaced relatively close together (10−500 mV) depending upon the R and R′ substituents.[9] As such, more than one mechanism is viable, including an ECEC pathway, whereby the first protonation follows reduction of the Ni^{II} complex to Ni^{I}, as well as an EECC process where the first protonation follows reduction of the catalyst to Ni^0 (Scheme 1).[14] The dominant pathway will depend on the relative rates of protonation for Ni^I versus Ni^0 and the separation of the $Ni^{II/I}$ and $Ni^{I/0}$ redox couples. A recent study of a $[Ni(P^R_2N^{R\prime}_2)_2]^{2+}$ successor, $[Ni(8P^{Ph}_2N^{C_6H_4Br})]$

Received: August 14, 2015
Published: October 9, 2015

DOI: 10.1021/jacs.5b08297
J. Am. Chem. Soc. 2015, 137, 13371−13380

Scheme 1. Proposed Catalytic Cycle Highlighting Both the ECEC and the EECC Pathways[a]

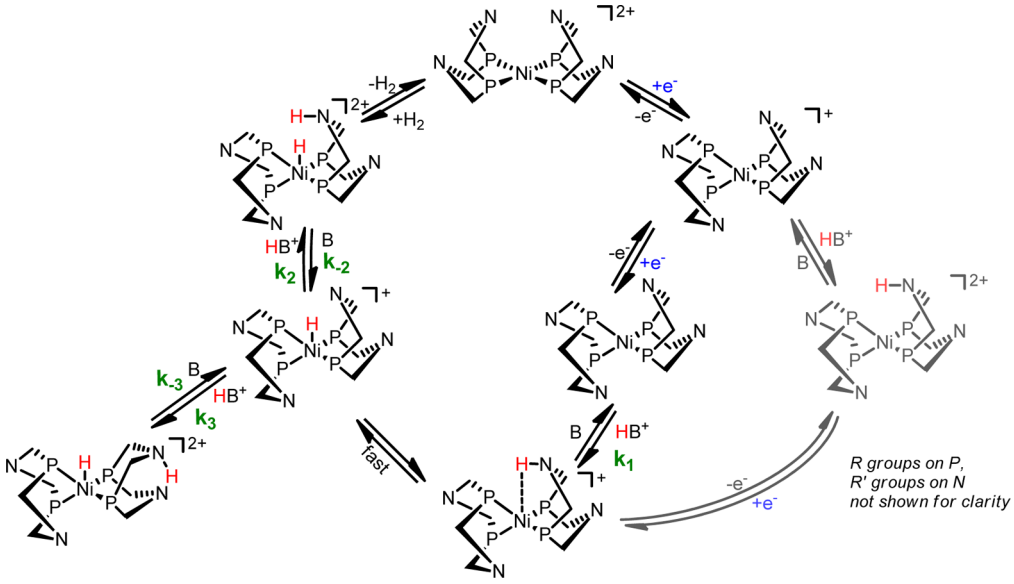

[a]The EECC pathway, the focus of this work, is highlighted. Specific elementary steps of interest are marked with their corresponding rate constants. Some steps expected to be of importance to the overall catalytic cycle, including those regarding exo protonation of Ni^{I} species, have been removed for clarity.[22]

($8P_2^{Ph}N^{C_6H_4Br}$ = 1-*para*-bromophenyl-3,7-triphenyl-1-aza-3,7-diphosphacycloheptane), utilizing [(DMF)H][OTf] as the proton source suggested that indeed these pathways operate in parallel.[21] Further, Raugei and co-workers recently revealed that for $[Ni(P_2^{Ph}N_2^{Ph})_2(CH_3CN)][BF_4]_2$ (Figure 1), the ECEC

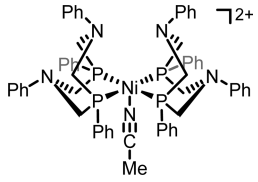

Figure 1. Structure of $[Ni(P_2^{Ph}N_2^{Ph})_2(CH_3CN)]^{2+}$.

and EECC pathways also operate in parallel.[14] In this report, it was predicted that if a proton source with the appropriate pK_a is used, the EECC pathway can be selectively promoted as the dominant operating pathway. In this work, we report that through judicious choice of acid, reactivity can indeed be tuned to promote the EECC pathway, allowing us to examine the reaction mechanism in the absence of competing phenomenon. Through a combination of electrochemical analysis and spectroscopy, rate constants for the elementary steps of this reaction pathway were determined, and an off-cycle intermediate was shown to limit the overall rate of catalytic turnover.

RESULTS

Electrocatalytic Response with Anilinium. The cyclic voltammogram (CV) of the $[Ni(P_2^{Ph}N_2^{Ph})_2]^{2+}$ complex exhibits two reversible, one-electron reduction waves, corresponding to the $Ni^{II/I}$ and $Ni^{I/0}$ couples, separated by 200 mV in acetonitrile (−0.83 and −1.03 V, all values reported versus $Fc^{+/0}$ couple, SI-1).[15] In a 1:1 dimethylformamidium:dimethylformamide (pK_a = 6.1)[23] acetonitrile solution, a large, yet nonideal (non-sigmoidal) catalytic response corresponding to the catalytic production of hydrogen is obtained (Figure 2).[14]

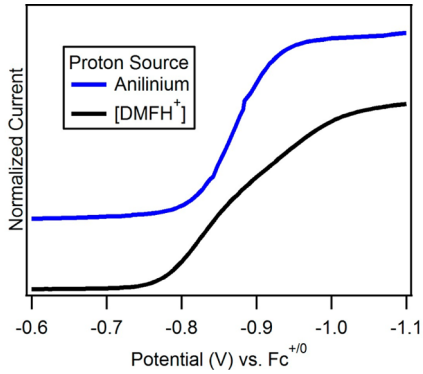

Figure 2. Electrocatalytic response obtained for $[Ni(P_2^{Ph}N_2^{Ph})_2]^{2+}$ (1 mM) with 1:1 [(DMF)H][BF_4]:[DMF] (70 mM, black) and with anilinium tetrafluoroborate (0.5 M, blue). The catalytic response with anilinium is a classical catalytic sigmoid, while with $(DMF)H^+$, the catalytic response has initial sigmoidal character and then changes slope ca. 150 mV prior to reaching a plateau. Voltammograms recorded at 100 mV/s in 0.2 M [NBu_4][PF_6] CH_3CN solutions.

By contrast, a more ideal sigmoidal catalytic response is obtained with anilinium (pK_a = 10.6)[23] as the proton source. When examining the voltammetric wave over a range of anilinium concentrations (Figure 3), three key observations are made.

(1) At low acid concentrations (2 and 4.1 mM), the $Ni^{II/I}$ wave remains unaltered, but a significant shift (ca. 100 mV) in the peak corresponding to the $Ni^{I/0}$ couple is observed. This peak continues to shift as the concentration of acid is increased. (2) As the concentration of acid is increased, the catalytic current deviates from an initial first-order response in acid[24] and approaches a zone where the catalytic plateau current is acid-independent. (3) Even after the current plateau becomes

DOI: 10.1021/jacs.5b08297
J. Am. Chem. Soc. 2015, 137, 13371−13380

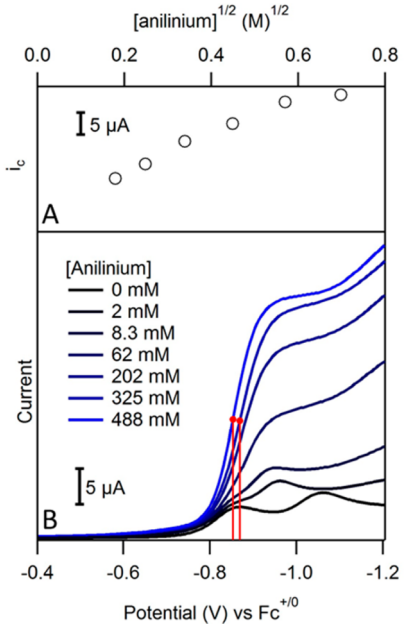

Figure 3. (A) The plateau current (i_c) plotted against the square root of the anilinium concentration exhibits the linear dependence anticipated for a reaction that is first order in acid up to ca. 360 mM anilinium. At higher concentrations, the current levels off. (B) Linear sweep voltammograms of 0.9 mM $[Ni(P^{Ph}_2N^{Ph}_2)_2]^{2+}$ with varied concentrations of anilinium tetrafluoroborate. For the two most concentrated solutions, $E_{cat/2}$ is marked to highlight the shift in potential. Voltammograms recorded at 100 mV/s in 0.2 M $[NBu_4][PF_6]$ CH_3CN solutions.

zero-order in acid, the half-wave potential for the catalytic sigmoid ($E_{cat/2}$) continues to shift positive with acid concentration.[24] Analysis of these three features provides key details of the mechanism and kinetics associated with catalytic hydrogen production.

Protonation of a Ni^0 Species To Form Ni^{II}–H. Upon the addition of 1 equiv of anilinium tetrafluoroborate to a solution of $[Ni(P^{Ph}_2N^{Ph}_2)_2]^{2+}$, a new oxidation feature is observed via CV at approximately −0.4 V (Figure 4). This stoichiometric acid addition does not lead to catalytic turnover, but was anticipated

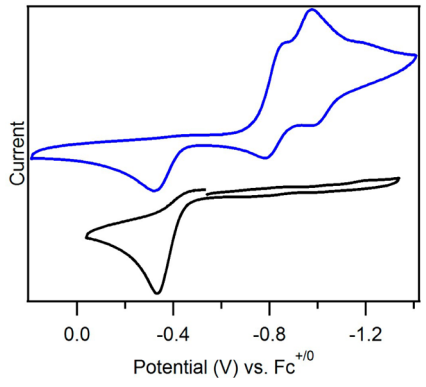

Figure 4. Cyclic voltammograms of 1.5 mM $[Ni(P^{Ph}_2N^{Ph}_2)_2]^{2+}$ and approximately 1 equiv of anilinium (blue) as compared to the cyclic voltammogram of 0.6 mM of the independently synthesized Ni^{II}–hydride (black) in CH_3CN. The new oxidation observed at −0.4 V for $[Ni(P^{Ph}_2N^{Ph}_2)_2]^{2+}$ in the presence of acid matches that of the isolated hydride. Voltammograms recorded at 100 mV/s in 0.2 M $[NBu_4][PF_6]$ CH_3CN solutions.

to promote formation of the Ni^{II}–H species, $[HNi(P^{Ph}_2N^{Ph}_2)_2]^{2+}$, upon protonation of the Ni^0 species formed electrochemically. To determine if the new peak observed corresponds to the oxidation of the Ni^{II}–H, the hydride complex was synthesized and evaluated independently.

$[HNi(P^{Ph}_2N^{Ph}_2)_2]^{2+}$ was prepared by addition of 1 equiv of of sodium borohydride to $[Ni(P^{Ph}_2N^{Ph}_2)_2]^{2+}$ in acetonitrile and is stable over a period of several days, provided it is kept under an inert atmosphere. The hydride peak in the ^1H NMR (SI-2) is observed as a quintet ($^2J_{PH}$ = 30.5 Hz) at −8.1 ppm,[15] consistent with related nickel(II)–hydride complexes, and the $^{31}P\{^1H\}$ singlet shifts from 6.6 to 17.4 ppm.[25−27] The CV of the synthesized hydride shows no redox activity at the $Ni^{II/I}$ and $Ni^{I/0}$ redox potentials of $[Ni(P^{Ph}_2N^{Ph}_2)_2]^{2+}$, but instead an irreversible oxidation is observed at approximately −0.4 V, confirming the assignment of the new oxidation wave observed in the CV of $[Ni(P^{Ph}_2N^{Ph}_2)_2]^{2+}$ and 1 equiv of acid (Figure 4). Increasing the scan rate did not produce any noticeable increase in reversibility up to 25 V/s.

Peak Shift Analysis. The rate constant for the protonation of the Ni^0 species $[Ni(P^{Ph}_2N^{Ph}_2)_2]$ was first determined by analyzing the peak shift of the $Ni^{I/0}$ redox wave as a function of acid concentration. While the $Ni^{I/0}$ wave quickly becomes buried under the catalytic wave as the acid concentration is increased, catalytic turnover is thwarted upon the addition of excess aniline (1 M), allowing the kinetics of protonation to be isolated. The peak shift ($E_P - E_{1/2}$) of the $Ni^{I/0}$ peak was recorded as a function of aniline concentration (0–306 mM) (Figure 5). While the ratio of aniline base to anilinium changes dramatically over the course of this titration, the peak location was shown to be unaffected by base concentration (see SI-3).

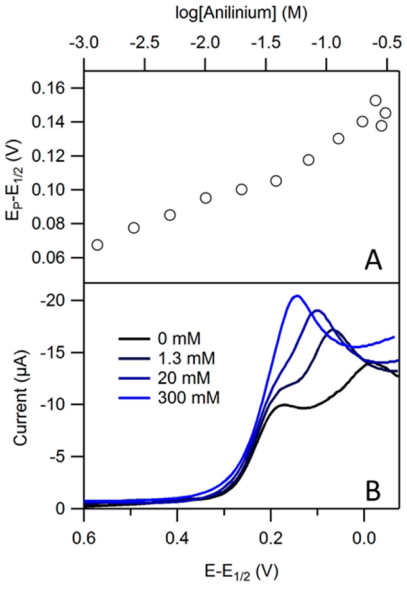

Figure 5. As a solution of 1 mM $[Ni(P^{Ph}_2N^{Ph}_2)_2]^{2+}$ containing 1 M aniline is titrated with anilinium tetrafluoroborate, the peak location of the $Ni^{I/0}$ reduction shifts positively with concentration. (A) Peak location at different concentrations of anilinium; the peak shifts 33 mV per decade, indicating an EC mechanism and giving a rate constant for hydride formation of 1.2×10^6 M^{-1} s^{-1}. (B) Linear sweep voltammograms at several concentrations of anilinium. Current is plotted versus ($E - E_{1/2}$), where $E_{1/2}$ corresponds to the reversible $Ni^{I/0}$ wave. Voltammograms recorded at 100 mV/s in 0.2 M $[NBu_4][PF_6]$ CH_3CN solutions.

DOI: 10.1021/jacs.5b08297
J. Am. Chem. Soc. 2015, 137, 13371−13380

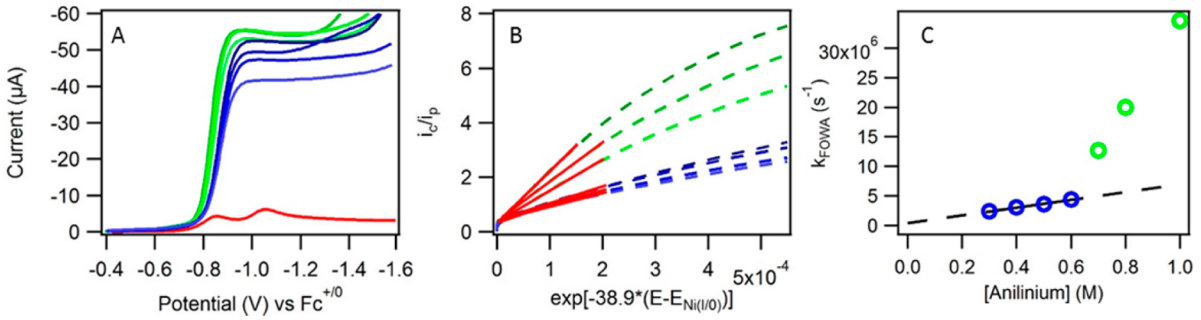

Figure 6. (A) Cathodic sweeps of catalytic cyclic voltammograms with 1 mM $[Ni(P^{Ph}_2N^{Ph}_2)_2]^{2+}$ and 0−1 M anilinium tetrafluoroborate. (B) For FOWA, the ratio of catalytic current to the noncatalytic peak current of the $Ni^{II/I}$ reduction is plotted versus $e^{-(F/RT)(E-E_{Ni(I/0)})}$ (F/RT = 38.9). The linear portion of the FOW plots was fit (red lines). (C) The pseudo-first-order rate constants obtained from the FOWA analysis. Rate constants for the 0.3−0.6 M anilinium data sets are shown as the blue data points and are fit to a line with a slope of 6.5 × 10^6, while those at higher concentrations (green) fit to a line with a much steeper slope that does not intercept the origin, signifying a change in mechanism, likely a shift from an EECC to ECEC. Voltammograms recorded at 50 mV/s in 0.2 M $[NBu_4][PF_6]$ CH_3CN solutions.

For an electrochemical EC mechanism, in which a Nernstian electron transfer is followed by an irreversible chemical step, the magnitude of the peak shift can be related to the rate constant for protonation under pseudo-first-order conditions per eq 2, where F is Faraday's constant, $[BH^+]$ is the concentration of anilinium, k_1 is the second-order rate constant for protonation, υ is the scan rate, T is temperature, and R is the ideal gas constant.[28,29]

$$E_p = E^0_{I/0} - \frac{RT}{F}(0.78) + \frac{RT}{2F}\ln\left(\frac{k_1[BH^+]RT}{F\upsilon}\right) \quad (2)$$

The relationship observed between peak shift and acid concentration (Figure 5) is consistent with eq 2, which predicts a slope of 30 mV/decade (observed slope is 33 mV/decade) and provides a rate constant for protonation of 1.2 × 10^6 M^{-1} s^{-1}.

Foot-of-the-Wave Analysis. As was mentioned previously (Figure 3), we observe that even after the current plateau loses its first-order dependence on anilinium concentration, the value of $E_{cat/2}$ continues to shift positive. This behavior is anticipated for EECC scenarios in which the first step of the catalytic cycle is not rate limiting; evaluation of the rate constant for this first step is possible through foot-of-the-wave analysis (FOWA).[20] This analysis offers many advantages over other methods to extract rate data; for instance, the kinetics can be analyzed at the earliest time-points in the experiment when only a small fraction of the catalyst is active so that inhibiting factors such as substrate depletion or product inhibition will have a minimal effect on the measurement.[20,24,30−32] Use of FOWA requires that several assumptions be made; the reaction must not be limited by heterogeneous electron transfer steps, substrate must be present in sufficient excess such that its depletion is not a factor at the foot of the wave, the catalyst does not degrade significantly on the time scale of the experiment, and in the case of a multistep reaction, the mechanism should be established prior to analysis.[20,30,32] For multistep catalytic reactions following an EECC-type mechanism, application of FOWA provides the pseudo-first-order rate constant for the first chemical step ($k_{FOWA} = k_1[BH^+]$) in the catalytic cycle via eq 3 (SI-4), where i_c refers to the current at potential E in the catalytic wave, D_{cat} is the diffusion coefficient of the catalyst, C_{cat} is the concentration of the catalyst, and A is the area of the working electrode.[20,24]

$$i_c = 2FAC_{cat}\sqrt{k_{FOWA}D_{cat}}\,\exp\left[-\frac{F}{RT}(E - E^0_{I/0})\right] \quad (3)$$

As the catalytic wave that originates for the $Ni^{I/0}$ couple overtakes the $Ni^{II/I}$ potential, the anticipated accuracy of FOWA analysis with an underlying redox wave was first investigated. It was shown to cause tolerable error in the calculation (see SI-5). After validating the extension of FOWA to our data, analysis of a series of voltammograms recorded with anilinium concentrations between 0.3 and 1 M (Figure 6A) was carried out to determine the rate constant for protonation of the Ni^0 species. The resulting voltammograms were then converted to the FOWA plot according to eq 4 (eq 3 divided by the Randles−Sevcik equation, SI-4, where n represents the number of electrons in the wave corresponding to i_p (the peak current of the $Ni^{II/I}$ reduction wave in the absence of catalyst)). The slope of the initial linear region (m) was then determined (Figure 6B), and the observed rate constant (k_{FOWA}) was calculated using eq 5 (see SI-4 for more details).

$$\frac{i_c}{i_p} = \frac{0.7179}{n}\sqrt{\frac{k_{FOWA}}{n\upsilon}}\,\exp\left[-\frac{F}{RT}(E - E^0_{I/0})\right] \quad (4)$$

$$k_{FOWA} = \left(\frac{m}{3.212}\right)^2 \quad (5)$$

A plot of k_{FOWA} versus concentration of anilinium (Figure 6C) reveals two distinct regions. At low concentrations of anilinium (0.3−0.6 M), linear regression provides a value for k_1 of 6.5 × 10^6 M^{-1} s^{-1}, while at higher acid concentrations, a steeper dependence is observed and the linear fit does not pass through the origin. This change in slope suggests a change in mechanism, likely from EECC at lower concentrations to ECEC at higher concentrations (see below). In this scenario, FOWA can be performed using the reduction potential for $Ni^{II/I}$ (see SI-4).

Reactivity of Ni^{II}−H. *Stopped-Flow Kinetics Analysis.* Reaction of the isolated Ni^{II}−H complex with anilinium to generate $[Ni(P^{Ph}_2N^{Ph}_2)_2]^{2+}$ was monitored using stopped-flow spectroscopy. As the bright yellow Ni^{II}−H has substantially distinct optical properties from the dark red $[Ni(P^{Ph}_2N^{Ph}_2)_2]^{2+}$ complex (Figure 7B), reaction kinetics were evaluated by optically monitoring the appearance of $[Ni(P^{Ph}_2N^{Ph}_2)_2]^{2+}$ (λ_{obs} = 500 nm) as a function of time (ms−s). The kinetics traces

DOI: 10.1021/jacs.5b08297
J. Am. Chem. Soc. 2015, 137, 13371−13380

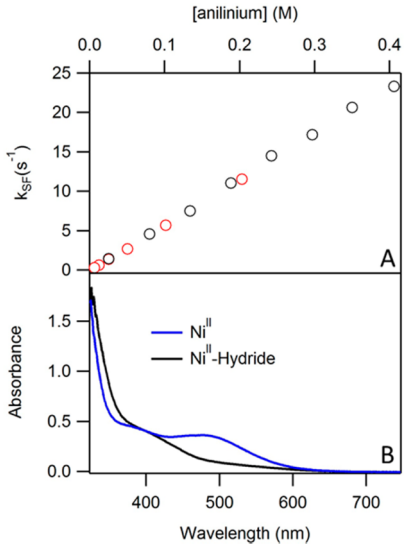

Figure 7. (A) Observed pseudo-first-order rate constant k_{SF} determined from stopped-flow kinetics studies versus anilinium concentration. The linear relationship provides a first-order rate constant of 58 M^{-1} s^{-1}. Red and black markers indicate data obtained from separate experiments. Experimental conditions: 0.2 mM $[HNi(P^{Ph}_2N^{Ph}_2)_2]^{2+}$. (B) Absorbance spectra of 0.36 mM $[Ni(P^{Ph}_2N^{Ph}_2)_2]^{2+}$ and $[HNi(P^{Ph}_2N^{Ph}_2)_2]^{2+}$ in CH_3CN.

recorded as a function of anilinium concentration (SI-6) under pseudo-first-order conditions ([anilinum] ≫ [Ni^{II}−H]) were fit with single exponential kinetics. The first-order rate constant k_{SF} is linearly dependent on anilinium concentration (Figure 7A) giving a second-order rate constant of 58 M^{-1} s^{-1} for the conversion of $[HNi(P^{Ph}_2N^{Ph}_2)_2]^{2+}$ to $[Ni(P^{Ph}_2N^{Ph}_2)_2]^{2+}$. On longer time scales (ca. 1−150 s), continued growth of $[Ni(P^{Ph}_2N^{Ph}_2)_2]^{2+}$ absorption was observed, suggesting a second process is necessary for full conversion. This second process could not be fit to single exponential kinetics, suggesting the involvement of an intermediate species generated during the reaction (SI-6). At all concentrations of anilinium, the short time scale kinetics accounted for conversion of ca. 88% of $[HNi(P^{Ph}_2N^{Ph}_2)_2]^{2+}$ to $[Ni(P^{Ph}_2N^{Ph}_2)_2]^{2+}$ (SI-6). In contrast to the protonation of the Ni^0 species, addition of aniline to the reaction solution causes the observed rate of the fast time scale reaction to slow significantly. Additionally, the slow kinetics regime is substantially elongated with base; after the initial fast kinetics regime, the absorption reaches a plateau, and then a slow conversion (~25 min) to $[Ni(P^{Ph}_2N^{Ph}_2)_2]^{2+}$ proceeds (SI-7). We attribute this to the reversibility of hydrogen formation in the presence of excess base (see below).

Kinetics Details Obtained from Electrocatalytic Plateau Currents. Catalytic voltammograms were recorded over a range of concentrations of anilinium. The overall rate constant for catalysis under steady-state electrocatalytic conditions was determined from the current plateau. For an EECC reaction, the plateau current (i_{pl}) is a function of the overall rate constant for catalysis (k_{pl}) as defined by eq 6.[20] The rate constant k_{pl} reflects the rate-limiting chemical step, or a composite of elementary steps, for electrocatalysis (see below). Dividing i_{pl} by i_p (peak current of the $Ni^{II/I}$ wave in the absence of catalysis) gives eq 7. Rearrangement of eq 7 provides an expression for k_{pl} (n = 1 and υ = 0.05 V/s, eq 8, SI-8). The overall rate constant plotted versus the anilinium concentration (Figure 8) reveals a first-order dependence on acid at low acid concentrations, but

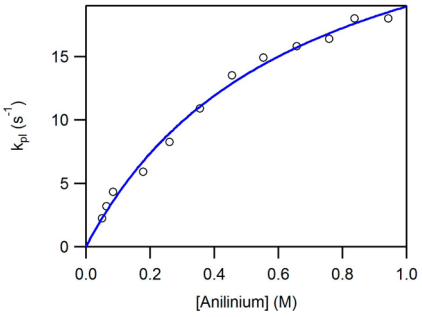

Figure 8. Observed rate constants obtained from the current plateau of catalytic voltammograms of 0.4 mM $[Ni(P^{Ph}_2N^{Ph}_2)_2]^{2+}$ (calculated using eq 8) versus anilinium concentration. Data points are fit with $k_{pl} = ((k_2k_{obs,-3}[BH])/(k_3[BH] + k_{obs,-3})$ with k_2 = 48 M^{-1} s^{-1}, k_3 = 12 M^{-1} s^{-1}, and $k_{obs,-3}$ = 8 s^{-1} (rate constants defined in Scheme 1 and discussed below; derivation of k_{pl} equation can be found in SI-10). Voltammograms recorded at 50 mV/s in 0.2 M $[NBu_4][PF_6]$ CH_3CN solutions.

k_{pl} approaches an acid-independent region as the concentration is increased, consistent with previous reports.[15,16,33,34]

$$i_{pl} = 2FAC_{cat}\sqrt{k_{pl}D_{cat}} \quad (6)$$

$$\frac{i_{pl}}{i_p} = \frac{4.48}{n}\sqrt{\frac{RTk_{pl}}{nF\upsilon}} \quad (7)$$

$$k_{pl} = \left(\frac{i_{pl}/i_p}{3.212}\right)^2 \quad (8)$$

Ni^{II}−H Reactivity in the Presence of Excess Aniline Examined via NMR. The long time scale reactivity of Ni^{II}−H observed in the stopped-flow experiments suggests the presence of a reaction intermediate; to probe this hypothesis, the reaction of Ni^{II}−H with 1 equiv of anilinium and 10 equiv of aniline was monitored by $^{31}P\{^1H\}$ NMR spectroscopy. With this large excess of base employed for these experiments, we obtained an equilibrium between the reactants, intermediates, and products as hydrogen formation is reversible in the presence of excess base.[15] Upon mixing, the singlet at 17.4 ppm corresponding to Ni^{II}−H decreases in intensity and a new resonance appears at 6.6 corresponding to $[Ni(P^{Ph}_2N^{Ph}_2)_2]^{2+}$ (SI-9). Assuming no degradation, integration of the peaks after equilibrium is established (6 h) shows that $[Ni(P^{Ph}_2N^{Ph}_2)_2]^{2+}$ accounts for 63% of the total nickel concentration. No additional species were identified by NMR, suggesting that the differences observed in the stopped-flow experiments (discussed above) upon the addition of excess base do not result from the creation of more of the anticipated intermediate.

DISCUSSION

Isolation of the EECC Mechanism. Work by Raugei and co-workers has shown that with relatively strong acids like $(DMF)H^+$, the Ni^I species formed upon reduction of $[Ni(P^{Ph}_2N^{Ph}_2)_2]^{2+}$ is protonated, promoting catalysis via an ECEC pathway at potentials near the $Ni^{II/I}$ reduction potential. As the potential approaches the $Ni^{I/0}$ wave, rapid electron transfer to generate Ni^0 outcompetes protonation of the Ni^I species and the EECC mechanism becomes competitive.[14,21] Computational studies suggest that the pK_a values of $[Ni(P^{Ph}_2N^{Ph}_2)_2H]^{2+}$ and $[Ni(P^{Ph}_2N^{Ph})H]^+$ differ by approximately

DOI: 10.1021/jacs.5b08297
J. Am. Chem. Soc. 2015, 137, 13371−13380

8 pK_a units, indicating that stronger acids are necessary to protonate the Ni^I species than the Ni^0 complex.[33] As such, it was reasoned that protonation of the Ni^I species could be averted by raising the pK_a of the acid employed for catalysis, allowing the more potential-intensive EECC mechanism to be isolated. Indeed, dramatic differences in catalytic response are observed for anilinium versus $(DMF)H^+$, indicating that the reaction pathway for hydrogen generation can be controlled by choice of proton source (Figure 2). The catalytic current responses observed upon the addition of low concentrations of anilinium further support the assertion that catalysis proceeds via an EECC mechanism with weak acids, as the catalytic wave grows off the $Ni^{I/0}$ reduction wave (Figure 3).

Kinetic Analysis of Protonation. In the EECC reaction pathway presented in Scheme 1, the $[Ni(P^{Ph}_2N^{Ph}_2)_2]^0$ complex formed upon two sequential electrochemical reductions of the Ni^{II} species is protonated to produce the Ni^{II}–H species $[HNi(P^{Ph}_2N^{Ph}_2)_2]^+$. Identification of this reaction intermediate is supported by comparison of the voltammetric features observed for $[Ni(P^{Ph}_2N^{Ph}_2)_2]^{2+}$ with substoichiometric acid to those of the independently synthesized hydride complex (Figure 4). Two methods were utilized to obtain the rate constant for protonation of the Ni^0 species, EC peak shift analysis and FOWA. The former afforded a rate constant of 1.2×10^6 M^{-1} s^{-1}, similar to the rate constant of 6.5×10^6 M^{-1} s^{-1} determined via FOWA at low acid concentration (0.3–0.6 M). We anticipate the small difference in rate constants may be due to differing effects of electron transfer kinetics on the two analyses. Notably, at higher acid concentrations (>0.6 M), the observed first-order rate constants calculated via FOWA are substantially higher than those determined at low acid concentrations. This observation is consistent with the assertion that two parallel mechanisms are operating. While protonation of the Ni^I species is not kinetically competitive at low anilinium concentrations, these data suggest that protonation of the singly reduced catalyst can compete at high concentration of this weak acid. When FOWA is performed at these higher acid concentrations assuming an ECEC pathway, a rate constant of 10 M^{-1} s^{-1} is estimated for the protonation of Ni^I by anilinium (see SI-4). While protonation of the Ni^0 species by anilinium is 5 orders of magnitude faster than the protonation of Ni^I, the concentration of Ni^I is much higher than Ni^0 at the potentials near the foot of the wave and thus protonation of the former can compete. For comparison, Wiedner et al. measured a rate constant of 3×10^5 M^{-1} s^{-1} for protonation of Ni^I with the much stronger proton source $(DMF)H^+$ by analyzing the current–potential relationship of the catalytic waves.[35] Artero and Saveant have previously estimated a similar value of k_1 for protonation by $(DMF)H^+$ (7.5×10^4 M^{-1} s^{-1}) via analysis of the plateau current and the $E_{1/2}$ value.[36]

Formation of an Off-Cycle Intermediate. Because protonation of the Ni^0 species occurs at a sufficiently rapid rate, we expected that a subsequent elementary step, such as protonation of Ni^{II}–H or H_2 release, would be rate limiting for catalytic turnover. As such, we anticipated that stopped-flow kinetics, which monitored the reformation of Ni^{II} upon protonation of Ni^{II}–H, and the electrochemical current plateau studies should yield the same observed rate constants because they both measure the conversion of $[HNi(P^{Ph}_2N^{Ph}_2)_2]^+$ to $[Ni(P^{Ph}_2N^{Ph}_2)_2]^{2+}$, provided the same mechanism is followed in each experiment. As is readily observed in Figures 7 and 8, the kinetics of the two experiments differ dramatically. For the cyclic voltammetry experiments, the observed rate constant is first order in acid at low acid concentrations, but saturates at higher acid concentrations with an overall rate constant of approximately 20 s^{-1}. By contrast, the stopped-flow kinetics remain first order in acid at all concentrations tested, even when observed rate constants exceed 20 s^{-1}. These differences can be interpreted by considering the various accessible protonation modes of $[HNi(P^R_2N^{R'}_2)_2]^{2+}$ complexes, which have been revealed through extensive experimental and computational study.[8,14,22,33,37–40] Protonation of Ni^I, Ni^0 and Ni^{II}–H can occur in endo or exo modes. In this experiment we are sensitive to the endo vs exo protonation of Ni^{II}–H (Figure 9). In the endo isomer, the pendant amine is protonated

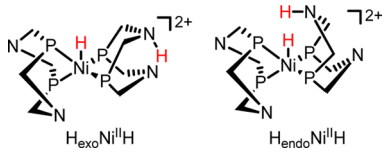

Figure 9. Endo versus exo protonation of $HNi(P^{Ph}_2N^{Ph}_2)_2$. Phenyl substituents on the phosphines and amines were omitted for clarity.

proximal to the metal center, while for the exo species the proton is "pinched" between two amines.[22] Studies have suggested that exo isomer ($H_{exo}Ni^{II}H$) is catalytically inactive and the species must be deprotonated and reprotonated to form the endo isomer to re-enter the catalytic cycle (Scheme 1).[39–41] The endo isomer ($H_{endo}Ni^{II}H$) is required for H_2 formation and catalytic turnover.

With this in mind, we examined how the formation of the catalytically inactive $H_{exo}Ni^{II}H$ species, an off-cycle intermediate, would influence the observed kinetics in both the stopped-flow and the cyclic voltammetry data in the proposed reaction cycle (Scheme 1, SI-10). As detailed below and in the Supporting Information, the production of Ni^{II} and H_2 upon reaction of the isolated Ni^{II}–H species with excess acid follows pseudo-first-order kinetics in the fast kinetic regime, the observed rate constant (k_{SF}) varying linearly with acid concentration. By contrast, the observed rate constant obtained from the plateau current of catalytic cyclic voltammograms ($k_{overall}$) will initially be first order in acid but become acid-independent at larger concentrations of acid. This major difference arises because Ni^{II}–H and $H_{exo}Ni^{II}H$ reach an equilibrium under catalytic conditions (as experienced in the reaction layer of the voltammetry experiment), and their concentrations are at steady state (the observation of a well-defined current plateau in the catalytic voltammograms is indicative of steady-state conditions), while this is not the case when monitoring the direct reaction of the isolated Ni^{II}–H $[HNi(P^{Ph}_2N^{Ph}_2)_2]^+$ with acid (as in the fast kinetic regime of the stopped-flow experiments)).

The stopped-flow experiments carried out monitor the appearance of $[Ni(P^{Ph}_2N^{Ph}_2)_2]^{2+}$ as a function of time. As proposed above, the Ni^{II} species is generated upon rapid release of H_2 from $H_{endo}Ni^{II}$–H, the latter formed by protonation of the $Ni^{II}H$.

$$Ni^{II}H + BH^+ \xrightarrow{k_2} H_{endo}Ni^{II}H + B$$

$$H_{endo}Ni^{II}H \xrightarrow{fast} Ni^{II} + H_2$$

DOI: 10.1021/jacs.5b08297
J. Am. Chem. Soc. 2015, 137, 13371–13380

Assuming release of H_2 from $H_{endo}Ni^{II}H$ is rapid,[18] the formation of Ni^{II} from Ni^{II}–H is governed by the protonation step, which is first order in both acid and Ni^{II}–H. The change in concentration of the Ni^{II} species as a function of time can be described per eq 9.

$$\frac{d[Ni^{II}]}{dt} = k_2[Ni^{II}H][BH^+] \quad (9)$$

However, the reversible protonation of Ni^{II}–H to form $H_{exo}Ni^{II}H$ must also be accounted for, which affects the concentration of Ni^{II}–H.

$$Ni^{II}H + BH^+ \overset{k_3}{\rightarrow} H_{exo}Ni^{II}H + B$$

$$H_{exo}Ni^{II}H + B \overset{k_{-3}}{\rightarrow} Ni^{II}H + BH^+$$

As detailed in the Supporting Information, consideration of the off-cycle intermediate in the kinetics analysis yields an observed rate constant under pseudo-first-order conditions ($[BH^+] \gg [Ni^{II}H]$) for the fast regime that is the sum of the rate constants for endo protonation (k_2) and exo protonation (k_3) times the acid concentration (eq 10).

$$k_{SF} = (k_2 + k_3)[BH^+] \quad (10)$$

Kinetics analysis of the catalytic voltammograms, by contrast, accounts for the steady-state concentrations of reaction intermediates generated under catalytic conditions. In this analysis, it is assumed that reduction of Ni^{II} to Ni^0 and subsequent protonation are both rapid; formation of Ni^{II} immediately results in the formation of Ni^{II}–H.

$$Ni^{II} + 2e^- + BH^+ \overset{fast}{\rightarrow} Ni^{II}H + B$$

$$Ni^{II}H + BH^+ \overset{k_2}{\rightarrow} H_{endo}Ni^{II}H + B$$

$$Ni^{II}H + BH^+ \overset{k_3}{\rightarrow} H_{exo}Ni^{II}H + B$$

$$H_{exo}Ni^{II}H + B \overset{k_{-3}}{\rightarrow} Ni^{II}H + BH^+$$

$$H_{endo}Ni^{II}H \overset{fast}{\rightarrow} Ni^{II} + H_2$$

A series of differential equations can be derived to describe the change in concentrations of Ni^{II}–H, $H_{exo}Ni^{II}H$, and H_2 as a function of time. Evaluating for the production of H_2 over time reveals an overall rate constant for catalysis that is dependent upon the rate constants for endo and exo protonation (k_2 and k_3) and the rate constant for deprotonation of $H_{exo}Ni^{II}H$ (k_{-3}). We thus determine that the rate constant k_{pl} determined from the catalytic CVs does not reflect a single rate-limiting step, but rather reflects the composite of rate constants describing the reactivity of the Ni^{II}–H. Stated otherwise, the second C in the EECC reaction does not reflect a single elementary step, but is a composite of the kinetics of the second protonation, release of hydrogen, and formation/deprotonation of exo species. It must be noted that to simplify the electrochemical analysis, the base dependence for deprotonation of $H_{exo}NiH$ was not included and is therefore represented in the equation as a first-order rate constant $k_{obs,-3}$. At low acid concentrations, k_{pl} is dependent on $[BH^+]$, while at high acid concentration, $k_3[BH^+] \gg k_{obs,-3}$, and the observed rate becomes acid independent.

$$k_{pl} = \frac{k_2 k_{obs,-3}[BH^+]}{k_3[BH^+] + k_{obs,-3}} \quad (11)$$

Equations 10 and 11 were applied to the stopped-flow and plateau current data, respectively, to determine rate constants k_2 and k_3. The relative values were obtained from stopped-flow by considering the total rate constant for protonation ($k_2 + k_3$, 58 M^{-1} s^{-1}, Figure 7) and the extent of conversion to Ni^{II} in the fast kinetics (SI-6). The observed 88% conversion to Ni^{II} in the fast kinetics predicts that k_2 is 7.3 times faster than k_3, giving a value for k_2 of 51 M^{-1} s^{-1} and a value for k_3 of 7 M^{-1} s^{-1}. Fitting the electrocatalytic plateau current (k_{pl} vs [anilinium], Figure 8) to eq 11 provided values of 48 M^{-1} s^{-1} for k_2 and 12 M^{-1} s^{-1} for k_3, similar to those obtained from stopped-flow analysis. The electrochemical data also give a value for $k_{obs,-3}$ of 8 s^{-1}, but, as noted above, this value holds little meaning as it should have a dependence on base concentration.

The second kinetic regime observed in the stopped-flow experiments (in the absence of excess base, see below), which leads to the complete conversion of $[HNi(P^{Ph}_2N^{Ph}_2)_2]^{1+}$ to $[Ni(P^{Ph}_2N^{Ph}_2)_2]^{2+}$, is congruent with the idea that the $H_{exo}Ni^{II}H$ intermediate must be converted back to an on-cycle intermediate before turnover. Attempts to spectroscopically detect this intermediate were not successful; both manual inspection and singular value decomposition (SI-11) of spectral traces at various time points after mixing revealed only a linear combination of $[Ni(P^{Ph}_2N^{Ph}_2)_2]^{2+}$ and $[HNi(P^{Ph}_2N^{Ph}_2)_2]^{1+}$ absorbance spectra, indicating that the $H_{exo}Ni^{II}H$ absorbance may be spectroscopically indistinguishable from these species. The reaction was also investigated by $^{31}P\{^1H\}$ NMR (SI-9, SI-13) in search of the third species, yet no reaction intermediate was detected.

A value for k_{-3} (100 M^{-1} s^{-1}, SI-12) was estimated by kinetics simulations of the stopped-flow traces; however, the values obtained were fairly inconsistent between data sets, suggesting the process is more complex than the simple deprotonation depicted in Scheme 1. For instance, it has been suggested that initial protonation in the exo position is followed by boat-to-chair isomerization to form the stabilizing "pinched" N–H–N hydrogen bond of the off-cycle intermediate.[18] The pK_as of these two species are expected to differ substantially; competing deprotonation of the two exo-protonated species, along with the kinetics of chair-boat isomerization, likely complicate the determination of rate constant k_{-3}.

Inspection of the mechanism presented in Scheme 1 suggests that addition of excess base to the reaction should accelerate catalysis by facilitating deprotonation of $H_{exo}Ni^{II}H$, and this should be reflected in the reaction kinetics observed via cyclic voltammetry. However, addition of aniline (conjugate base of anilinium) reduces the catalytic current (SI-14). Further, the addition of aniline in stopped-flow experiments results in a significant decrease of the observed rate constant k_{SF} and a decrease in the percent conversion to $[Ni(P^{Ph}_2N^{Ph}_2)_2]^{2+}$ in the fast kinetic regime (SI-7). We posit that aniline rapidly deprotonates the $H_{endo}Ni^{II}H$ species before H_2 can be released. Excess of aniline also causes the long time scale kinetics to slow, rather than speed up as would be predicted if base facilitates deprotonation of the off-cycle intermediate $H_{exo}Ni^{II}H$. To probe the effects of base further, the reactivity of the Ni^{II}–H with anilinium in the presence of excess base was examined via $^{31}P\{^1H\}$ NMR. With 1 equiv of anilinium and 10 equiv of aniline, the reaction approached an equilibrium between the

DOI: 10.1021/jacs.5b08297
J. Am. Chem. Soc. 2015, 137, 13371–13380

Ni^{II} species and the Ni^{II}–H. The $H_{exo}Ni^{II}H$ species was not detected.

Together, these data suggest that the production of hydrogen in the presence of excess aniline inhibits the reaction of the Ni^{II}–H with acid to produce H_2 from reaching completion. On the basis of the propensity of these nickel species to heterolytically cleave H_2 in the presence of base, we conclude that the equilibrium established between the Ni^{II} species and the Ni^{II}–H in the presence of excess base results from this process. Under this equilibrium, effusion of hydrogen from the solution would be required for the reaction to proceed to completion. By contrast, when no base is added to the reaction solution, the evidence suggests that the longer time scale kinetics do not reflect the reversibility of hydrogen release and cleavage, as the concentration of anilinium, which should influence this equilibrium, has no effect on the extent of reaction. At all anilinium concentrations, the fast time scale kinetics account for 88% of the conversion, as would be expected if two species (Ni^{II} and $H_{exo}Ni^{II}H$) were formed simultaneously in processes that are first order in anilinium. Rather, the long time scale kinetics likely reflect the deprotonation of the $H_{exo}NiH$ species to reform $Ni^{II}H$, which can lead to productive H_2 evolution. Exploring the details of these elementary reaction steps is the focus of our ongoing investigations.

The equilibrium reached between $[Ni(P^{Ph}_2N^{Ph}_2)_2]^{2+}$ and $[HNi(P^{Ph}_2N^{Ph}_2)_2]^{+}$ in the presence of excess aniline provides an opportunity to estimate the rate constant k_{-2}. Using the value of k_{-3} determined from analysis of the long time scale stopped-flow kinetics, the equilibrium between $H_{exo}Ni^{II}H$, Ni^{II}–H, and Ni^{II} was examined. With this value of k_{-3}, no $H_{exo}Ni^{II}H$ species should be spectroscopically detectable as the equilibrium between Ni^{II}–H and $H_{exo}Ni^{II}H$ should afford approximately 300 times the concentration of the former over the latter under the given conditions, consistent with experimental observations. A value of k_{-2} (1.5×10^4 M^{-2} s^{-1}) was also estimated from the equilibrium established (SI-13). The value is provided as a third-order rate constant, but the conversion from $[Ni(P^{Ph}_2N^{Ph}_2)_2]^{2+}$ to $[HNi(P^{Ph}_2N^{Ph}_2)_2]^{2+}$ likely occurs in two elementary steps (Scheme 1), hydrogen binding followed by proton abstraction.[15] As such, the third-order rate constant is not a true rate constant for an elementary step, but rather reflects the rate of proton abstraction from the hydrogen bound $H_{endo}Ni^{II}H$ species, which is in equilibrium with the Ni^{II} complex.

CONCLUSIONS

The $[Ni(P^{R}_2N^{R'}_2)_2]^{2+}$ class of molecules and their successors[8,21] are some of the most successful hydrogen evolution catalysts to date. A great deal of effort has gone into the study of what makes them so efficient and fast, including thermodynamic,[22] kinetic,[15] structural,[7] and environmental[37] aspects. This has opened the door for researchers to make use of these complexes as tools for both technique development and application-based research.[42] In this work, investigations of $[Ni(P^{Ph}_2N^{Ph}_2)_2]^{2+}$ illustrate the ability to control the reaction mechanism by judicious choice of proton source pK_a. The elementary steps of catalysis were then examined. Electrochemical methodology, specifically peak shift analysis and foot-of-the-wave analysis, provided the rate constant for protonation of the Ni^0 species. Electrochemistry, stopped-flow spectroscopy, and NMR spectroscopy were all used in concert to interpret the rest of the catalytic pathway beyond hydride formation. The mechanism, as we have postulated and consistent with past proposals,[22] is shown in Scheme 1. Rate constants for elementary steps determined from these analyses are presented in Table 1. Good agreement was found across techniques for the values of k_1, k_2, and k_3. Because of experimental limitations, the values for k_{-2} and k_{-3} were determined by a single technique each.

Table 1. Rate Constants Determined for Elementary Reaction Steps of Hydrogen Production Catalyzed by $[Ni(P^{Ph}_2N^{Ph}_2)_2]^{2+}$

	k_1 (M^{-1} s^{-1})	k_2 (M^{-1} s^{-1})	k_{-2} (M^{-2} s^{-1})	k_3 (M^{-1} s^{-1})	k_{-3} (M^{-1} s^{-1})
EC	1.2×10^6				
FOWA	6.5×10^6				
stopped-flow		51		7	100
current plateau		48		12	
NMR			1.5×10^4		

This work contributes to our understanding of the $[Ni(P^{R}_2N^{R'}_2)_2]^{2+}$ catalysts, especially by confirming that catalysis is initiated by hydride formation and that the zero-order acid dependence observed in catalytic voltammograms at high acid concentrations is a result of biasing the formation of an off-cycle intermediate $H_{exo}Ni^{II}H$. Perhaps more importantly, this work illustrates the importance of extending beyond electrochemical methods for examining catalytic reaction pathways and evaluating reaction kinetics. The in-depth study of the Ni^{II}–H reactivity by stopped-flow kinetic analysis has presented a platform for detailed analysis of the effect of proton source on hydrogen evolution catalysis, work that is currently underway in our laboratory. The agreement we have found between the stopped-flow and electrochemical measurements, along with other studies of its kind,[32] should instill confidence for use of both methods in future studies of electrocatalysts.

EXPERIMENTAL SECTION

General Materials and Methods. Molecular synthesis was performed under N_2 either on a Schlenk line or in an inert-atmosphere glovebox. Acetonitrile (Fisher Scientific, HPLC grade, >99.9%) and diethyl ether (Fisher Scientific, >99%) were degassed with argon and dried using a Pure Process Technology solvent system. Aniline (Sigma-Aldrich) was degassed using a freeze–pump–thaw technique and stored in the inert-atmosphere glovebox. Dimethylformamide was degassed with N_2 and stored in the inert-atmosphere glovebox. Tetrabutylammonium hexafluorophosphate (TCI, >98%) was recrystallized from hot ethanol, filtered, washed with cold ethanol, and dried at room temperature under vacuum overnight. Nickel powder (Sigma-Aldrich) and phenylphosphine (Alfa Aesar) were used as received. Dimethylfomamidium triflate,[43] anilinium tetrafluoroborate,[23] and $[Ni(P^{Ph}_2N^{Ph}_2)_2(CH_3CN)][BF]_2$[15] were prepared by literature methods. NMR spectra were recorded on either a Bruker 400 MHz spectrometer (characterization) or a Bruker 600 MHz spectrometer (kinetics). ^1H NMR were referenced to proteo solvent impurities, and ^{31}P and $^{31}P\{^1H\}$ were referenced to a standard of phosphoric acid. Simulations for mechanistic interpretation were performed in MATLAB (MathWorks) using differential equation solver ode45 or ode23s (SI-12). UV–vis absorption measurements were taken on an Agilent Cary 60 UV–vis spectrophotometer using 1 cm path length quartz cuvettes.

Preparation of Ni^{II}–H ($[HNi(P^{Ph}_2N^{Ph}_2)_2]^{+}$). To a stirred acetonitrile solution (~1 mL) of $[Ni(P^{Ph}_2N^{Ph}_2)_2]^{2+}$ (5.5 mg, 4.7 μmol) was added 76 μL of a 60.8 mM solution of sodium borohydride (1 equiv).

DOI: 10.1021/jacs.5b08297
J. Am. Chem. Soc. 2015, 137, 13371–13380

Subsequently, the solvent and residual BH_3 were removed under vacuum. The resulting yellow solid was then dissolved in ~0.5 mL of deteurated acetonitrile. NMR suggested 100% conversion (SI-2). ^{1}H NMR (CD_3CN, 400 MHz): δ −8.1 (quintet, $^2J_{PH}$ = 30.5 Hz, NiH). $^{31}P\{^1H\}$ NMR (CD_3CN, 160 MHz): δ 17.4 (s).

Electrochemistry. Electrochemical experiments were performed under a nitrogen atmosphere in an inert atmosphere glovebox using dry acetonitrile with 0.2 M $[Bu_4N][PF_6]$ electrolyte on a Pine Instruments WaveDriver potentiostat with a silver wire pseudoreference separated from the main solution by a glass frit, a glassy carbon counter electrode, and a 3 mm disk glassy carbon working electrode. A freshly polished working electrode was used for every voltammogram recorded. Electrodes were polished before experiments with 0.05 μm alumina powder (CH Instruments, contained no agglomerating agents) Milli-Q water slurries. They were then rinsed and sonicated to remove residual alumina. Before measurements were taken, electrodes were pretreated by scanning two cycles from 1 to −2 V (vs Ag wire) at 400 mV/s in electrolyte solution.[23] In a generic catalysis experiment, a stock solution of $[Ni(P^{Ph}_2N^{Ph}_2)_2(CH_3CN)][BF_4]_2$ and ferrocene (internal reference) was prepared (both ~1 mM), and then two separate, equal volume, solutions were prepared using the stock solution: one that only contained $[Ni(P^{Ph}_2N^{Ph}_2)_2(CH_3CN)][BF_4]_2$ and another that contained the same concentration of catalyst and an acid. The cyclic voltammetric response of the catalyst only was measured, and then the solution containing the acid was titrated in over ~10 additions. A similar procedure was performed for the peak shift experiments; the stock solutions also contained 1 M in aniline. All scans were referenced to the ferrocene/ferrocenium couple post data collection. The direct reduction of anilinium is sufficiently negative on glassy carbon such that it should not interfere in the analyzed region.[23]

Stopped-Flow Experiments. Stopped-flow experiments were performed on a Hi-Tech Scientific SF-61 DX2 double mixing stopped-flow in single mixing mode with Kinetic Studio data acquisition software (v2.33). Single wavelength kinetics measurements were taken using a dual reference/main PMT setup with a tungsten lamp. Spectra measurements were taken using a photodiode array with a xenon lamp. Stopped-flow measurements were all performed under an N_2 atmosphere. This was accomplished by preparing solutions inside an inert-atmosphere glovebox in septum-sealed bottles. A solution of $[HNi(P^{Ph}_2N^{Ph}_2)_2]^+$ (0.2−0.5 mM) was prepared by dissolving $[Ni(P^{Ph}_2N^{Ph}_2)_2]^{2+}$ in approximately 10 mL of acetonitrile, and then 1 equiv of sodium borohydride was added and the solution was diluted to 25 mL. Stock solutions of anilinium were also prepared. PEEK tubing was used to transfer solutions directly from sealed bottles to the stopped flow syringes to avoid exposure to air. To ensure purity, the syringe was purged three times with each solution prior to each measurement. In a typical experiment, one syringe was loaded with the $[HNi(P^{Ph}_2N^{Ph}_2)_2]^+$ solution, and the other was loaded with the anilinium solution of the desired concentration. Upon injection, absorbance versus time was monitored at 500 nm. Fitting of the resulting traces was performed using a single exponential in Igor Pro 6.34A Software. The residual borane was shown through control reactions to not affect the stopped-flow kinetics (SI-15).

NMR Equilibrium. Nine milligrams of $[Ni(P^{Ph}_2N^{Ph}_2)_2(CH_3CN)][BF_4]_2$ was dissolved in 1 mL of deuterated acetonitrile (5 mM). A 0.5 mL aliquot was removed, and a $^{31}P\{^1H\}$ NMR was taken. One equivalent of $NaBH_4$ was then added to generate the hydride in situ in the remaining 1 mL. Separately, 1 mg of anilinium BF_4 (5 mM) and 5 μL of aniline (50 mM) were dissolved in 25 mL of acetonitrile. 0.5 mL of the hydride solution and 0.5 mL of the anilinium:aniline solution were placed in a J. Young air-free NMR tube. $^{31}P\{^1H\}$ NMR spectra were obtained for each of the three solutions after allowing equilibrium to be established (equilibrium is established in approximately 2 h, SI-13; however, spectra were recorded at 6 h).

■ ASSOCIATED CONTENT

Supporting Information

The Supporting Information is available free of charge on the ACS Publications website at DOI: 10.1021/jacs.5b08297.

Characterization data for $[HNi(P^{Ph}_2N^{Ph}_2)_2]^+$, derivations of all equations within the text, control experiments, and additional cyclic voltammograms and stopped-flow spectra (PDF)

■ AUTHOR INFORMATION

Corresponding Author

*dempseyj@email.unc.edu

Notes

The authors declare no competing financial interest.

■ ACKNOWLEDGMENTS

We thank Brian McCarthy, Dr. Monte Helm, Dr. Eric Wiedner, Dr. Morris Bullock, Dr. Aaron Appel, and Dr. Simone Raugei for insightful discussions. B.M. is also thanked for his help with the graphical abstract. The lab of Prof. Thomas Meyer is gratefully acknowledged for the use of their stopped-flow instrumentation, and Dr. Rob Binstead is thanked for training and assistance. Alexander Ullman is gratefully acknowledged for experimental contributions during early parts of this study. This work was supported by the University of North Carolina at Chapel Hill. E.S.R. was supported by a Richard G. Hiskey Graduate Fellowship.

■ REFERENCES

(1) Costentin, C.; Robert, M.; Savéant, J.-M. *Chem. Soc. Rev.* **2013**, *42*, 2423−2436.

(2) Bullock, R. M.; Appel, A. M.; Helm, M. L. *Chem. Commun.* **2014**, *50*, 3125−3143.

(3) Dempsey, J. L.; Brunschwig, B. S.; Winkler, J. R.; Gray, H. B. *Acc. Chem. Res.* **2009**, *42*, 1995−2004.

(4) Wasylenko, D. J.; Palmer, R. D.; Berlinguette, C. P. *Chem. Commun.* **2013**, *49*, 218−227.

(5) Concepcion, J. J.; Jurss, J. W.; Brennaman, M. K.; Hoertz, P. G.; Patrocinio, A. O. T.; Murakami Iha, N. Y.; Templeton, J. L.; Meyer, T. J. *Acc. Chem. Res.* **2009**, *42*, 1954−1965.

(6) Wilson, A. D.; Shoemaker, R. K.; Miedaner, A.; Muckerman, J. T.; DuBois, D. L.; DuBois, M. R. *Proc. Natl. Acad. Sci. U. S. A.* **2007**, *104*, 6951−6956.

(7) Rakowski DuBois, M.; DuBois, D. L. *Chem. Soc. Rev.* **2009**, *38*, 62−72.

(8) Helm, M. L.; Stewart, M. P.; Bullock, R. M.; DuBois, M. R.; DuBois, D. L. *Science* **2011**, *333*, 863−866.

(9) Kilgore, U. J.; Stewart, M. P.; Helm, M. L.; Dougherty, W. G.; Kassel, W. S.; Dubois, M. R.; Dubois, D. L.; Bullock, R. M. *Inorg. Chem.* **2011**, *50*, 10908−10918.

(10) DuBois, D. L. *Inorg. Chem.* **2014**, *53*, 3935−3960.

(11) DuBois, D. L.; Bullock, R. M. *Eur. J. Inorg. Chem.* **2011**, *2011*, 1017−1027.

(12) Yang, J. Y.; Bullock, R. M.; DuBois, M. R.; DuBois, D. L. *MRS Bull.* **2011**, *36*, 39−47.

(13) Rakowski DuBois, M.; DuBois, D. L. *Acc. Chem. Res.* **2009**, *42*, 1974−1982.

(14) Ho, M.-H.; Rousseau, R.; Roberts, J. A. S.; Wiedner, E. S.; Dupuis, M.; DuBois, D. L.; Bullock, R. M.; Raugei, S. *ACS Catal.* **2015**, *5*, 5436−5452.

(15) Wilson, A. D.; Newell, R. H.; McNevin, M. J.; Muckerman, J. T.; Rakowski DuBois, M.; DuBois, D. L. *J. Am. Chem. Soc.* **2006**, *128*, 358−366.

(16) Pool, D. H.; DuBois, D. L. *J. Organomet. Chem.* **2009**, *694*, 2858−2865.

DOI: 10.1021/jacs.5b08297
J. Am. Chem. Soc. 2015, 137, 13371−13380

(17) Ginovska-Pangovska, B.; Dutta, A.; Reback, M. L.; Linehan, J. C.; Shaw, W. J. *Acc. Chem. Res.* **2014**, *47*, 2621−2630.
(18) Hou, J.; Fang, M.; Cardenas, A. J. P.; Shaw, W. J.; Helm, M. L.; Bullock, R. M.; Roberts, J. A. S.; O'Hagan, M. *Energy Environ. Sci.* **2014**, *7*, 4013−4017.
(19) Stewart, M. P.; Ho, M.; Wiese, S.; Lindstrom, M. Lou; Thogerson, C. E.; Raugei, S.; Bullock, R. M.; Helm, M. L. *J. Am. Chem. Soc.* **2013**, *135*, 6033−6046.
(20) Costentin, C.; Savéant, J.-M. *ChemElectroChem* **2014**, *1*, 1226−1236.
(21) Wiese, S.; Kilgore, U. J.; Ho, M.-H.; Raugei, S.; DuBois, D. L.; Bullock, R. M.; Helm, M. L. *ACS Catal.* **2013**, *3*, 2527−2535.
(22) Chen, S.; Ho, M.; Bullock, R. M.; DuBois, D. L.; Dupuis, M.; Rousseau, R.; Raugei, S. *ACS Catal.* **2014**, *4*, 229−242.
(23) McCarthy, B. D.; Martin, D. J.; Rountree, E. S.; Ullman, A. C.; Dempsey, J. L. *Inorg. Chem.* **2014**, *53*, 8350−8361.
(24) Rountree, E. S.; McCarthy, B. D.; Eisenhart, T. T.; Dempsey, J. L. *Inorg. Chem.* **2014**, *53*, 9983−10002.
(25) Das, P.; Stolley, R. M.; van der Eide, E. F.; Helm, M. L. *Eur. J. Inorg. Chem.* **2014**, *2014*, 4611−4618.
(26) Wiedner, E. S.; Yang, J. Y.; Chen, S.; Raugei, S.; Dougherty, W. G.; Kassel, W. S.; Helm, M. L.; Bullock, R. M.; Rakowski DuBois, M.; DuBois, D. L. *Organometallics* **2012**, *31*, 144−156.
(27) Galan, B. R.; Sch, J.; Linehan, J. C.; Seu, C.; Appel, A. M.; Roberts, J. A. S.; Helm, M. L.; Kilgore, U. J.; Yang, J. Y.; Dubois, D. L.; Kubiak, C. P. *J. Am. Chem. Soc.* **2011**, *133*, 12767−12779.
(28) Nicholson, R. S.; Shain, I. *Anal. Chem.* **1964**, *36*, 706−723.
(29) Bard, A. J.; Faulkner, L. R. In *Electrochemical Methods: Fundamental and Applications*, 2nd ed.; Harris, D., Swain, E., Robey, C., Aiello, E., Eds.; John Wiley & Sons, Inc.: Hoboken, 2001.
(30) Costentin, C.; Drouet, S.; Robert, M.; Savéant, J.-M. *J. Am. Chem. Soc.* **2012**, *134*, 11235−11242.
(31) Elgrishi, N.; Chambers, M. B.; Fontecave, M. *Chem. Sci.* **2015**, *6*, 2522−2531.
(32) Wasylenko, D. J.; Rodríguez, C.; Pegis, M. L.; Mayer, J. M. *J. Am. Chem. Soc.* **2014**, *136*, 12544−12547.
(33) Fraze, K.; Wilson, A. D.; Appel, A. M.; DuBois, M. R.; DuBois, D. L. *Organometallics* **2007**, *26*, 3918−3924.
(34) Kilgore, U. J.; Roberts, J. A. S.; Pool, D. H.; Appel, A. M.; Stewart, M. P.; DuBois, M. R.; Dougherty, W. G.; Kassel, W. S.; Bullock, R. M.; DuBois, D. L. *J. Am. Chem. Soc.* **2011**, *133*, 5861−5872.
(35) Wiedner, E. S. Unpublished work; Pacific Northwest National Laboratory: Richland, WA, 2015.
(36) Artero, V.; Saveant, J.-M. *Energy Environ. Sci.* **2014**, *7*, 3808−3814.
(37) Hoffert, W. A.; Roberts, J. A. S.; Morris Bullock, R.; Helm, M. L. *Chem. Commun.* **2013**, *49*, 7767−7769.
(38) O'Hagan, M.; Shaw, W. J.; Raugei, S.; Chen, S.; Yang, J. Y.; Kilgore, U. J.; DuBois, D. L.; Bullock, R. M. *J. Am. Chem. Soc.* **2011**, *133*, 14301−14312.
(39) Smith, S. E.; Yang, J. Y.; Dubois, D. L.; Bullock, R. M. *Angew. Chem., Int. Ed.* **2012**, *51*, 3152−3155.
(40) O'Hagan, M.; Ho, M.; Yang, J. Y.; Appel, A. M.; DuBois, M. R.; Raugei, S.; Shaw, W. J.; DuBois, D. L.; Bullock, R. M. *J. Am. Chem. Soc.* **2012**, *134*, 19409−19424.
(41) Horvath, S.; Fernandez, L. E.; Appel, A. M.; Hammes-Schiffer, S. *Inorg. Chem.* **2013**, *52*, 3643−3652.
(42) Moore, G. F.; Sharp, I. D. *J. Phys. Chem. Lett.* **2013**, *4*, 568−572.
(43) Favier, I.; Duñach, E. *Tetrahedron Lett.* **2004**, *45*, 3393−3395.

DOI: 10.1021/jacs.5b08297
J. Am. Chem. Soc. 2015, 137, 13371−13380